Early View publication on wileyonlinelibrary.com
(issue and page numbers not yet assigned;
citable using Digital Object Identifier – **DOI**)

Phys. Status Solidi C, 1–6 (2011) / **DOI** 10.1002/pssc.201000399

physica status solidi c
www.pss-c.com
current topics in solid state physics

Optically active substoichiometric Si_3N_4 μ-cavities

Federico Ferrarese Lupi[*,1], Daniel Navarro-Urrios[1], Josep Monserrat[2], Carlos Dominguez[2], Paolo Pellegrino[1], and Blas Garrido[1]

[1] MIND-IN2UB, Dept. Electrònica, Universitat de Barcelona, C/ Martí i Franquès 1, 08028 Barcelona, Spain
[2] IMB-CNM, CSIC, Bellaterra, 08193 Barcelona, Spain

Received 6 June 2010, revised 27 October 2010, accepted 29 October 2010
Published online 2 February 2011

Keywords Si_3N_4, microcavity resonator, photoluminescence, optical loss

* Corresponding author: e-mail fferrarese@el.ub.es, Phone: +34 93 4039175, Fax: +34 93 4021148

We report on the morphological and emission properties of microdisk resonators with an optically active disk material made of luminescent substoichiometric Si_3N_4 matrix. We demonstrate the importance of optimising the material by finding a compromise between the photoluminesce properties and optical losses. A careful design of the cavities for optimising the radiative quality factors has been also performed, enabling us to produce active disks with low intrinsic losses. Subnanometer whispering gallery mode (WGM) resonances have been experimentally detected, showing quality factors as high as 1200 around the wavelength of 719 nm. These values are among the highest previously reported values in Si-nanocluster-based systems and are actually limited by the spectral resolution of our experimental setup. In addition, an increasing of the pumping flux is not generating a spectral widening of the resonances, thus not affecting the quality of the cavities. This is in contrast to what observed in other reports of Si-nc based microcavities, where significant enlargements are observed associated to carrier absorption losses.

1 Introduction One of the main relevant challenges in optoelectronics concerns the inexpensive integration of efficient light sources on a silicon-based circuit by using complementary metal-oxide semiconductor (CMOS) compatible approaches [1].
An interesting strategy is to combine the light emission properties of Si nanostructures (Si-nc), which is several orders of magnitude more efficient than bulk Si [2], and the optical properties of μ-cavities. In this context, active μ-resonator circular cavities (such as disks or rings) could generate a great impact not only in the short scale telecommunications application area but also in other fields like contamination and biochemical sensing.
Few works in the literature address such active microcavities, where Si-nc are present within a SiO_2 matrix [3-6]. While in Ref. [3] the low quality factors reported were associated to inhomogenous line broadening due to the slight dispersion of microdisk diameters within the excited area, in Refs. [4-6] quality factors between 1000 and 3000 were measured. However, at least for the two latter works, carrier absorption mechanisms decreased them dramatically with pump flux.
To the best of our knowledge, as an active medium for microdisk resonators, substoichiometric silicon nitrides (SRSN) has been only studied for applications in the IR region of the spectrum, [7,8] aiming to exploit the sensitization effect when Er^{3+} ions are present in the matrix.
However, SRSN systems have also revealed efficient light emission in the visible range [9], which could provide alternative routes towards the fabrication of optically active Si devices that need to be explored. In addition, the relatively low barrier mismatch between Si and Si_3N_4 makes this material suitable for efficient electrical excitation [10].
From the point of view of the passive photonic properties, SRSN materials present refractive indices higher than n=2, which allows producing highly performing compact devices deposited over SiO_2 cladding layers.
In this work we address the design and experimental characterisation of a system composed by an SRSN active disk deposited over a SiO_2 cladding layer, aiming to provide a better understanding of the characteristics and potentialities of this active cavity as a CMOS compatible light source.

We have initially followed two parallel guidelines:
(i) The design and simulation of the μ–disks, which has involved the study of their modal structure (Section 2).
(ii) A characterisation and optimisation of the active material in terms of its photoluminescence (PL) intensities (Section 3.2) and the optical losses measured in waveguides (Section 3.3)
Using optimised recipes for both the active materials and cavity morphologies we have finally fabricated active μ-disks. In Section 3.4, we present an experimental characterization of single μ–disks by means of visible μ-PL measurements.

2 Simulation results The simulated spectral analysis of the μ-disks has been made by using of a three-dimensional Finite Difference Time Domain method (FDTD) package [11]. We have analysed the position of the resonance peaks and electric field spatial distribution of the different whispering gallery modes (WGM) inside the cavity, which are modified by varying the structural parameters of the optical element (radius, disk height and cladding thickness).
The aim of this study was to obtain monomodal behaviours in the vertical direction (perpendicular to the disk surface) for the TE polarisation (parallel to the disk surface) with quite high free spectral ranges (*FSR*) and radiative quality factors (Q_{rad}) higher than 10^4. The spectral region of interest was around 0.7 μm, where the experimental PL emission of the active material was present (see Fig. 4).
In Fig. 1 we show the results for Q_{rad}, which decreases with the wavelength as a consequence of a confinement factor lowering of the supported modes. In addition, Q_{rad} increases with the disk radius, just reflecting the fact that the bending losses of the supported modes decrease.
It is also worth noting that we have optimised the disk thickness to be 0.3 μm, showing a maximum confinement factor while staying monomodal in the vertical direction.
The Q_{rad} results are several orders of magnitude higher than what would be expected for equivalent designs using substoichiometric SiO_2 as an active material. This is a consequence of a much lower refractive index with respect to SRSN and would prevent producing compact substoichiometric SiO_2 cavities over SiO_2.
Considering the technical limits of the experimental μ-PL setup that will be described in the following, it is difficult to experimentally study a cavity in which high order radial families are showing intense contributions.
Resonators with radii around 4 μm are a good compromise between high Q_{rad} values of the 1st radial family modes and low contribution of higher order radial families.

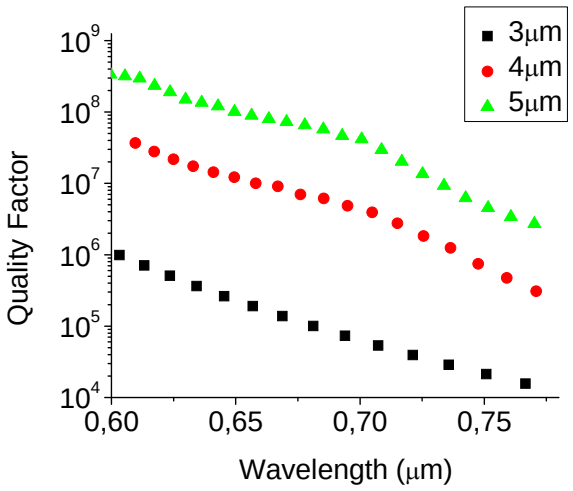

Figure 1 Spectral dependence of the quality factor associated to the 1st order radial family modes. Values corresponding to μ-disks of different radii (3, 4 and 5 μm) are reported.

As an example, in Fig. 2 we show the PL spectral dependence (TE polarization) of a 3 μm disk. Two different radial families are present, the fundamental one being much more intense and narrower than the second order one, which would be hardly observable experimentally. For the shortest wavelengths reported on the graph a third order radial family is also supported weakly. It is worth to note that the modes order has been confirmed by checking their spatial energy distribution.

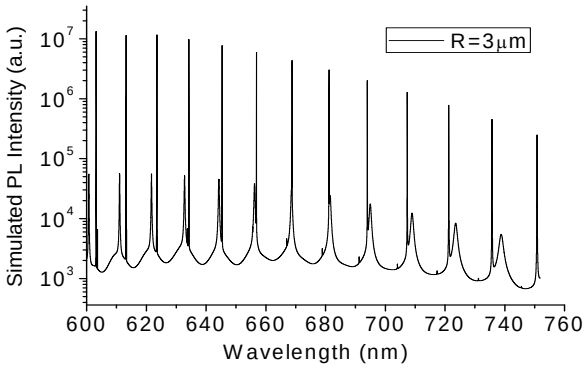

Figure 2 Simulated on plane PL emission for a disk of R=3 μm.

3 Sample characterisation

3.1 Sample preparation The samples under analysis have been produced using standard CMOS compatible processes. As a first step, 2 μm of SiO_2 was deposited on top of crystalline silicon wafers, acting as an optical cladding for the resonators. A layer of stoichiometric Si_3N_4 material has been subsequently deposited by using the LPCVD deposition technique, which has afterwards suffered a double ion implantation of Si followed by an an-

nealing procedure in N_2 atmosphere at 1100 ºC. The double implantation has been realised with the aim of obtaining a flat Si excess profile (see left panel of Fig. 3). We have performed EFTEM measurements on sample 1 and it was not possible to observe the formation Si nanocrystals within the active material. For the sake of clarity, we will only show results on two samples belonging to a wider set, labelled as sample 1 and 4 (see Table 1).

Sample	Si3N4 Thickness (nm)	Implantation energy (keV)	Implantation Dose (x10^{17} at / cm^2)	Annealing threatment
1	300	150 / 90	1.25 / 0.48	1100 ºC for 4h
4	300	150 / 90	0.62 / 0.24	1100 ºC for 4h

Table 1 Implantation parameters for samples 1 and 4.

As it is shown in Fig. 3, the limitation in the available implantation energy makes the Si-excess distribution to be centred slightly over the gravity centre of the fundamental mode at 660 nm, which is not the optimised situation in order to couple as much light as possible to the supported modes (whose gravity centre is displaced slightly towards the SiO_2 cladding).

The photonic structures have been defined by means of standard photolithographic techniques. In particular, we have designed disks with radius from 3 μm to 10 μm and waveguides with variable width (1-10 μm) for the characterisation of the optical losses. On the basis of what stated in Section 2, the disks have a thickness of 0.3 μm.

The surface analysis with AFM has revealed a very good top surface without inhomogeneities or irregularities (see Fig. 3). The roughness results to be on average lower than 1 nm, so we can neglect this source of optical losses.

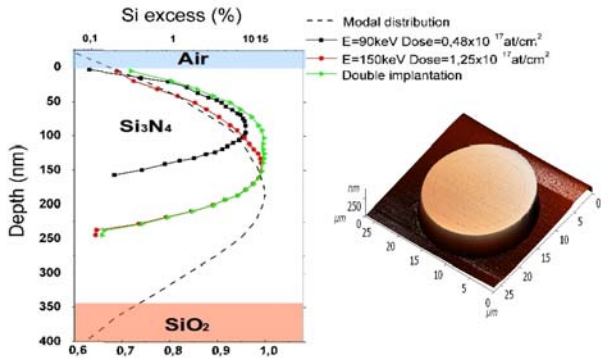

Figure 3 Left. Cross section of the device structure, implantation profile and modal energy distribution. Right. AFM analysis of a disk of radius 10 μm.

3.2 Standard PL characterisation Standard PL measurements were performed using the 488 nm line of an Ar laser. We have characterised and compared the PL emission properties of a of bulk region of active material on samples 1 and 4. Stoichiometric samples were not showing any PL.

Figure 4 shows the normalised spectra of both samples. A strong interference pattern is observed with a relatively short free spectral range (60-90 nm), which is related to the presence of a 2 μm thick SiO_2 cladding layer in addition to the 0.3 μm of Si_3N_4 material that the light has to travel before it is reflected backwards by the Si substrate.

In any case, it is clear that a red-shift of the PL maximum is observed when the Si implantation dose is increased.

In Fig. 5 we analyse, for those samples, the PL intensity and its evolution as a function of the pumping photon flux (Φ). It is observed that the PL intensity for sample 1 is about 1.8 times that of sample 4, almost scaling with the implantation dose. It is also interesting to note that the behaviour with Φ is linear, which means that, at least for this flux range, there are no flux dependent non-radiative recombination mechanisms (such as Auger-like processes) competing with the spontaneous emission process.

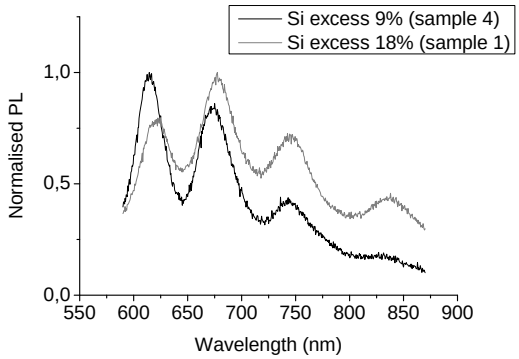

Figure 4 Normalised PL emission for samples 1 (gray) and 4 (black).

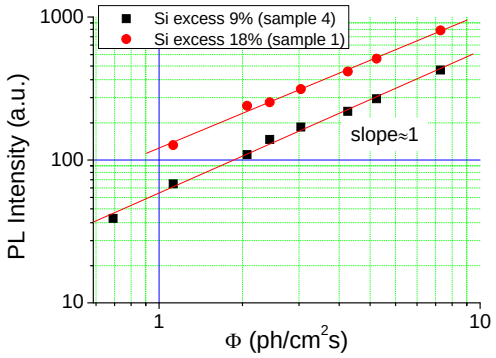

Figure 5 Integrated PL emission as a function of the photon flux for both samples.

3.3 Optical losses in rib-waveguides In this section we will describe the optical losses results in the visible region for both samples. We have used both the Cut-back and the Scattered Light Collection techniques.
The comparison between the results of these two samples shows a dramatic increase in optical losses with the amount of Si excess inside the Si_3N_4 matrix. Sample 1 could not be analysed by the cut-back technique because the intensity of transmitted light was well below the sensitivity limit. As it is shown in Fig. 6 for different waveguide widths, sample 4 presented acceptable propagation losses of about 6 dB/cm and 15 dB of coupling losses. Propagation losses below 1 dB/cm were determined on stoichiometric (not implanted) Si_3N_4 waveguide samples, which allow us to affirm that losses are increasing with Si excess in the matrix.

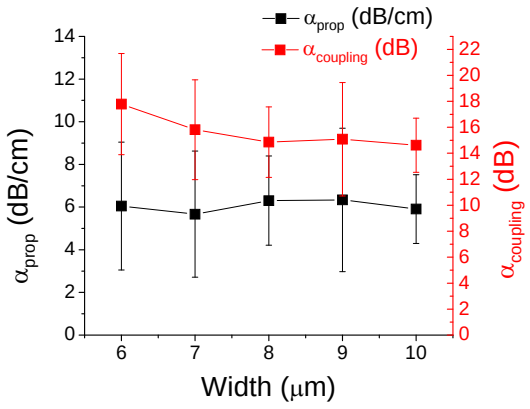

Figure 6 Propagation and coupling losses in VIS region (780 nm) for different waveguide widths for sample 1.

To overcome the limits arising from the cutback technique on sample 1, we performed measurement of the scattered light at 633 nm. By using this technique values close to 200 dB/cm for propagation losses in sample 1 have been detected. In view of application of the analysed material it is important to compare these results with that of Section 3.2: even if sample 1 presents higher PL intensity, it shows propagation losses values that will strongly deteriorate the total quality factor (Q) of an eventual cavity.
It is also worth noting that on sample 4 there is a propagation losses increase of about 10 dB/cm when moving from 780 to 633 nm, and that at 1.55 μm they were as low as 1 dB/cm (the lower detection limit of our setup).
The physical origin of the measured propagation losses is directly related with the amount of Si excess in the matrix. Since losses are decreasing with wavelength, we believe that they are probably a consequence of a combination between Rayleigh scattering from Si nanoclusters and direct absorption losses from the species that are likely generating the PL emission

3.4 μ-PL characterisation Room temperature μ-PL measurements have been performed by pumping with the 488 nm line of an Ar laser. A long working distance objective was used to focus the laser beam on the samples, having the possibility of a single resonator excitation since the spot can reach a diameter as small as 5 μm.
Low resolution measurements (~ 2 nm) have been performed in order to study the *FSR* and the distribution of resonance peaks. On the other hand, to extract the Q values, high resolution measurements were done (~ 0.6 nm).
Even if the PL intensity was higher for sample 1, the WGM of the disks were hardly appreciable. This is an expected result explained on the basis of the high propagation losses reported for this sample in the previous section. On the contrary, sample 4 presented strong WGM resonances, as it can be seen on the low resolution spectrum of Figure 8 (R = 4 μm).
Thus, it appears clear that, since the physical geometry and surface quality of the disks are independent on the implantation dose, the observation of WGM on sample 4 and not on sample1 is related to the significant difference of the optical losses reported for the waveguide devices.
We have compared the obtained μ-PL spectra with the results of the FDTD simulations. At this point it is worth to remember that the *FSR* is defined by:

$$FSR = \frac{\bar{\lambda}^2}{2\pi R n_g} \qquad (1)$$

where R is the radius of the disk, $\bar{\lambda}$ is the average wavelength in vacuum between the two resonance peaks and n_g is the group refractive index.
The agreement between simulations and experiment can be checked by comparing the results obtained for the FSR (extracted by determining the position of each resonant peak) and the extracted n_g (dashed curves of bottom and top panel respectively of Fig. 7).
It is also worth to note that an increase of the disk radius is reflected on a FSR reduction (in agreement with Eq. (1)), that results in a group refractive index insensitive to the disk radius, which is also consistent with performed simulations. The extracted n_g is thus compatible with what expected on the simulations for a Si_3N_4 like material. The uncertainty of the resonance positions translates in non-negligible variations of the extracted n_g, which prevents us to extract conclusions about the effect of the implantation on the material refractive index.
For the case of a 5 μm radius disk there is a slight disagreement between experiments and simulations. This is due to the fact that, in this case, also the second radial family is well supported. Thus, in the experiments, we are observing the superposition of resonances of the first two radial families, effectively resulting in an enlargement and shifting of the peaks and a false decrease of *FSR* (increase of the n_g) with respect to the real one for the first family.

On the other hand the total quality factor (Q) can be expressed as follows:

$$Q=2\pi\frac{n_g}{\lambda\alpha}=\frac{\lambda}{\Delta\lambda} \quad (2)$$

where α are the overall optical loss coefficient of the propagating mode.

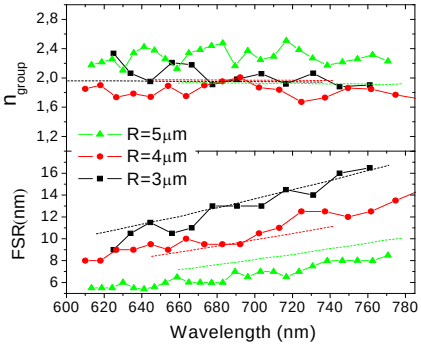

Figure 7 Bottom panel. FSR for the different disks reported together with simulations of the results for a 3 μm disk. Top panel. Group refractive index determined by using Eq. (2). Simulated results are reported as dashed lines.

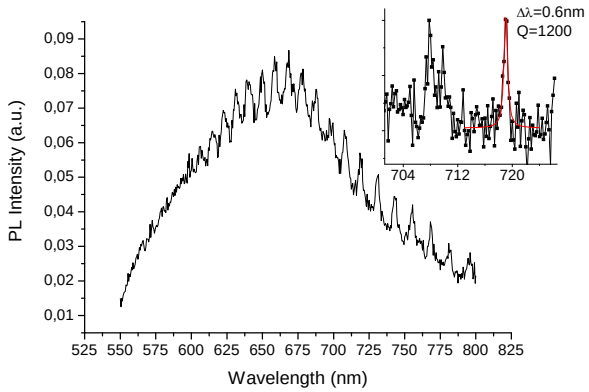

Figure 8 Main Panel. Low resolution μ-PL spectrum of a 4μm radius microdisk. Inset. High resolution spectrum of a particular part of the spectrum. The red curve shows a Lorentzian fit of one of the resonances.

The inset of Fig. 8 shows a restricted part of the spectrum acquired at the resolution limit of the experimental setup (narrowest slit widths). In this configuration we obtain $\Delta\lambda$ = 0.6 nm (equal to the minimum resolution), establishing a lower bound of Q = 1200 at λ_o = 719 nm.

We have also observed that the spectral width of the resonances broadens as the wavelength decreases until the resonances even disappear. This result is in contrast with the simulated behavior of Q_{rad}, which was decreasing with wavelength (see Fig. 1). We believe that this experimental behaviour is related with an increasing of the material optical losses at lower wavelengths. This is confirmed by our observation of different optical losses in the waveguide devices for 633 nm and 780 nm, where much higher losses were reported for the former wavelength on sample 4.

Furthermore, we can decompose Q in four different contributions, as follows:

$$Q^{-1}=Q_{rad}^{-1}+Q_{mat}^{-1}+Q_{ssc}^{-1}+Q_{sa}^{-1} \quad (3)$$

where the inverse of Q_{rad} , Q_{mat} , Q_{ssc} and Q_{sa} are related to radiation, material (bulk absorption and propagation), surface scattering and surface absorption losses, respectively.

As it was previously mentioned, AFM measurements performed on sample 4 show a high quality of the surface and shape of the disk, so we can neglect the last two terms in Eq. (3). Q_{rad} is related to the disk geometry and has been calculated by means of FDTD simulations to be greater than $Q_{rad} > 10^5$ for 4 μm disks. On the other hand, Q_{mat} is directly related to the material losses at the resonance wavelength, which we have already determined to be lower than 10 dB/cm, which means a $Q_{mat} \approx 10^5$. However, if we invert Eq. (2), we can extract an experimental value of α larger than 600 dB/cm. Therefore the 0.6 nm width of the observed resonances is effectively limited by the spectral resolution of our system, and not by the quality of the device, which might be as high as $Q \approx 10^5$.

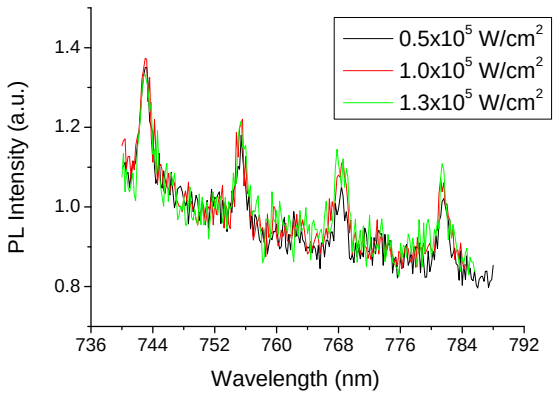

Figure 9 Different highly resolved spectrum obtained at different pump photon fluxes.

Moreover, we have performed experiments for different photon fluxes in order to check if there are flux induced losses. This behaviour is typical of carrier absorption mechanisms, not present in the absence of an external excitation mechanism [12]. In Fig. 9, we report the results obtained for a restricted region of the spectrum for different pump densities, where no broadening is detected.

4 Conclusions In conclusion, we have made a comprehensive study of active substoichiometric Si_3N_4 μ-disk resonators, where, on the one hand we have designed and optimised the photonic structure and on the other hand we

have studied the optical properties of the active material in order to find a compromise between PL intensity and optical losses.
Both studies have been combined in order to fabricate high quality disk resonators from the morphological and optical point of view. In fact we have demonstrated quality factors as high as 1200 at around 720 nm, actually limited by our setup resolution (about 0.6 nm in the best case).
Finally we have demonstrated that increasing the pumping flux does not generate a measurable spectral widening of the resonances, related to carrier absorption phenomena.

Acknowledgements The authors kindly acknowledge R. Guider and N. Prtljaga for helping in the morphological characterisation, and the Spanish Projects SENA (TSI-020301-2008-11), GICSERV (NGG-172) and LASSI (TEC 2008-08359) for financial support.

References

[1] L. Pavesi and D. J. Lockwood (eds.), Silicon Photonics (Springer, Berlin, 2004).
[2] L. Pavesi, S. Gaponenko, and L. Dal Negro (eds.), Towards the First Silicon Laser, NATO Advanced Studies Institute, Series 11, Vol. 93 (Kluwer Academic, Dordrecht, 2003).
[3] R.-J. Zhang, S.-Y. Seo, A. P. Milenin, M. Zacharias, and U. Gösele, Appl. Phys. Lett. **88**, 153120 (2006).
[4] A. M. Beltaos and A. Meldrum, J. Lumin. **126**, 607 (2007).
[5] M. Ghulinyan, D. Navarro-Urrios, A. Pitanti, A. Lui, G. Pucker, and L. Pavesi, Opt. Express **16**, 13218-13224 (2008).
[6] R. D. Kekatpure and M. Brongersma, Nano Lett. **8**, 3787-3793 (2008).
[7] Jee Soo Chang, Seok Chan Eom, Gun Yong Sung, and Jung H. Shin, Opt. Express **17**, 22918 (2009).
[8] J. H. Shin, M.-Se. Yang, J.-S. Chang, S.-Y. Lee, K. Suh, H. G. Yoo, Y. Fu, and P. Fauchet, Proc. SPIE **6897**, 68970N (2008).
[9] L. Dal Negro, J. H. Yi, J. Michel, L. C. Kimerling, T. F. Chang, V. Sukhovatkin, and E. H. Sargent , Appl. Phys. Lett. **88**, 233109 (2006).
[10] J. Warga, R. Li, S. Basu, and L. Dal Negro, Appl. Phys. Lett. **93**, 151116 (2008).
[11]A. Farjadpour, D. Roundy, A. Rodriguez, M. Ibanescu, P. Bermel, J. D. Joannopoulos, S. G. Johnson, and G. W. Burr, Opt. Lett. **31**, 2972 (2006).
[12] D. Navarro-Urrios, A. Pitanti, N. Daldosso, F. Gourbilleau, R. Rizk, G. Pucker, and L. Pavesi, Appl. Phys. Lett. **92**, 051101 (2008).

